Physically-Based Realistic Fire Rendering

Vincent Pegoraro[1] and Steven G. Parker[1]

[1] Scientific Computing and Imaging Institute, School of Computing, University of Utah
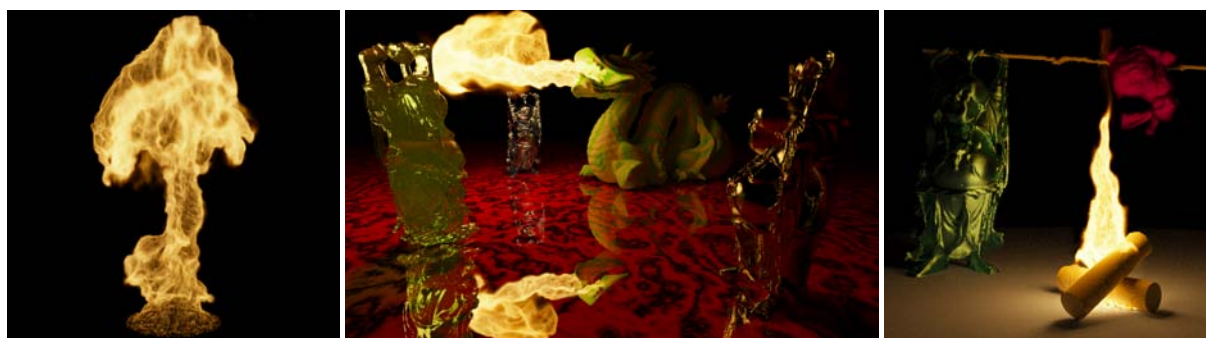

Figure 1: *Simulation of a methane pool fire, a fully path-traced scene where the flame is the unique light source, and a scene where refraction effects cause the straight wood stick to appear warped, all rendered using our physically-based fire rendering technique*

Abstract

Accurately rendering fires is a challenging problem due to the various subtle ways in which the electromagnetic waves interact with this complex participating medium. We present a new method for physically-based rendering of flames from detailed simulations of flame dynamics which accounts for their unique characteristics. Instead of relying on ad-hoc models, we build on fundamental molecular physics to compute the spectrally dependent absorption, emission and scattering properties of the various chemical compounds found in the fire. Combined with a model of the refractive process, and with tone-mapping techniques simulating the visual adaptation of a human observer, we are able to generate highly realistic renderings of various types of flames, including colorful flames containing chemical species with very characteristic spectral properties.

Categories and Subject Descriptors (according to ACM CCS): I.3.7 [Computer Graphics]: Three-Dimensional Graphics and Realism - Ray-tracing

1. Introduction

Humans have long had a fascination with fire due to its appealing appearance but dangerous nature. Flames are also important in many fields both in science and in computer graphics. They are a standard effect in the movie industry, but are typically filmed from actual fires with significant danger and expense. Computer-generated examples include Star Trek II [Par82] which made use of the first particle based technique developed by [Ree83], as well as the more recent animation movie Shrek, in which the technique described in [LF02] was used to model and render the flames. Applications have also emerged in several other sectors including the video-game industry, high fidelity virtual archaeological reconstructions [DC01, Cha02], as well as the development of safety oriented research. For instance, [BS97]

developed a simulation based design environment in order to help conceive building fire safety systems and evaluate the performance of building designs. Our work is similarly motivated by the desire to predict the visual appearance of a simulated flame to aid in the understanding of scientific simulations of fires and explosions.

Despite these vast applications, flame rendering still represents a challenging problem in computer graphics. This is due to the fact that fire is an extremely complex medium which hosts numerous simultaneous chemical and radiative processes. Most of the work done in this area has consequently been relying on simplified models addressing solely flames of yellow appearance, sometimes sacrifying accuracy and/or visual quality to achieve interactivity.

We propose a new method that provides physically-based simulation of the radiative energy transfer occurring in the participating medium. Starting with volumetric fields of temperature and species concentrations typically generated by computer simulation, we calculate the emissive properties of the flame using theoretical foundations in the domains of molecular chemistry and radiative physics, which are combined with algorithms from the computer graphics community. By investigating atomic and molecular characteristics, we are able to compute the spectral properties of the different chemical species. A model of the radiative transfer in the fire then allows to predict the radiant energy reaching a given observer. To enhance realism, we account for the non-linear propagation of the electromagnetic waves through the medium having a spatially varying index of refraction. Finally, a model of the visual adaptation mechanism via S-shape cone response is used to reproduce the signals that a real human observer would experience. This method is both flexible and robust in the sense that it allows for a truthful rendering of any type of fire without relying on any hand-tuned parameter. These include typical yellow flames dominated by soot radiation, as well as colorful flames where radiation from other specific chemical species prevails, and which to our knowledge has not been previously addressed in the computer graphics and visualization community.

This document starts by providing an overview of the techniques previously developed using diverse technologies. Then, we discuss the theoretical core on which our method is based, followed by a presentation of the implementation-specific issues and assumptions. We finally conclude by providing some visual results rendered using our technique, along with a discussion of the performance characteristics.

2. Previous Work

In this section, we present an overview of the former methods used for fire rendering, while making a distinction between raster-based and ray-tracing techniques. A more detailed survey is given in [ENM99].

2.1. Raster-based Techniques

[Ree83] first introduced particle systems to model and render fuzzy objects such as fire, where the particles are motion blurred in order to avoid temporal aliasing or strobing. [Sim90] extended this idea to a data parallel method used to render large numbers of particles. More recently, [CMTM94] developed a 2D model later extended to 3D by [TTC97], where both methods use a system of independent particles. Images are produced by rendering a motion-blurred primitive around each particle trajectory over a time step. [PP94] proposed an enhanced particle system where each particle consists of a set of non-overlapping coplanar triangles arranged to approximate a circle. By setting the transparency of the outer vertices to lower values, this method aims at eliminating the pointillistic artifacts inherent

to particle rendering. In [LKMD01], a simple point primitive is used to render the particles where the color and transparency of each particle is determined by the distribution of mass and size. Later, [IK03] presents an extension to the classical particle system, where a second order particle system is used to model the dynamics of the fire. [AH05] subsequently proposed to render the particles to the p-buffer of a programmable graphics card creating a cumulative blur to represent the scattering of particle light by hot gaseous products of combustion. Because of their discrete discontinuous nature, particle based methods are more suitable for real-time display than realistic rendering.

[WLMK02] and [ZWF*03] use texture splats as display primitives. While the former uses a black body color table to define the colors at different layers from the center of the fire, both model the radiative transfer properties by means of a simple alpha blending. [IR02] models and renders the fire by means of a perturbation map and a base map which allows for interactive frame rates but still gives little concern to the fidelity of the rendering. To achieve real-time animations, [BLLR06] models the flame shape using NURBS surfaces on which a transparent 2D texture is mapped.

[MK02] employs volume rendering, suitable for voxelized data, where the level of transparency is determined by the density in the voxel. The fuel gas is mapped to yellow and the flame front, where the reaction occurs, is mapped to red. [Has02, HK03, IM04] employed a tomographic method for reconstructing a volumetric model from multiple images of a fire. These algorithms provide realistic renderings but require that the same set-up be produced in a real environment and captured, which prevents a predictive capability.

2.2. Ray-tracing Techniques

[Ina90] proposed a simple laminar candle flame model based on a physical model of light emission and transmission in the regions of combustion. Rendering is achieved by applying a texture map to a flame-like implicit primitive which is then volume-traced. [Rac96] extended this work to include the dynamic nature of the flame. Later, [BPP01] developed a technique where a full fire is represented as a combination of individual primitive flames. For a single flame, implicit surfaces describe successive layers having a shape similar to the flame outline, each layer being a volume that emits light of a particular color and intensity. These methods imply some degree of simplicity in the spatial features of the fire being rendered, and are consequently not suitable for high frequency details that contribute to the realism of a fire rendering.

[Rob01] presents an image-based method modeling a candle flame as a set of spheres. This technique is restricted to phenomena producible in a real environment and imposes geometrical constraints. [LF02] uses a reference photograph mapped onto the profile used for the flame shape. The opacity of a particle is then estimated to be proportional to the relative brightness between itself and objects behind it.

[FOA03] shows flames arising from explosions that are generated by rendering the fuel and soot particles directly, but where the mapping is adjusted manually to match images of real explosions. [SF93], followed by [SF95], developed a new rendering technique using blob warping. A diffusion approximation is used to resolve the effects of multiple scattering, which are subsequently rendered using a blob tracer. The transparency along an interval due to a single blob is computed as a function only of the distance of the ray to the center of the blob and the endpoints of the interval.

An attempt to physically-based rendering was made by [RHC95] that discusses ray casting performed on measured data using a radiation path integration software [Gro95]. The computation is performed in terms of radiance units and combined with appropriate perceptual transformations to produce a true color image. A similar approach was followed by [NFJ02] which computes the radiance using the radiative transport equation and Planck's formula of blackbody radiation. Chromatic adaptation is finally modeled via white-point mapping. However, it doesn't consider the spectrally dependent properties of the various chemical compounds of the flame, and ignores the refraction process.

3. Physically-Based Realistic Rendering

In this section, we present our new physically-based rendering method and the theoretical background on which it builds. Since our algorithm accounts for the main chemical, physical and biological phenomena responsible for the visual response experienced by a real observer, our model is able to generate enhanced realistic fire renderings from first principles. To the best of our knowledge, our model is also the first that predicts the appearance of fires where radiation from colorful species prevails instead of the common blackbody emissions from soot particles.

3.1. Fire Modeling

While several of the references cited in the previous section address methods for modeling and animating fire, most of them do not accurately model the dynamics or radiations in the fire. However, the quality of a physically-based rendering depends inherently on the quality of the data representing the physical entities of interest.

For this reason, we use a model built on physically-based accurate simulations. Such a model has been developed by the Center for the Simulation of Accidental Fires and Explosions (C-SAFE) [HMS*00], which is focused on providing state-of-the-art, science-based tools for the numerical simulation of accidental fires and explosions, especially within the context of handling and storage of highly flammable materials. The primary objective of C-SAFE is to help to better evaluate the risks and safety issues associated with fires and explosions. A description of the combustion and radiation models used is given in [KBR*05] while implementation,

verification and validation of the radiation models are discussed in [KRS05] and [Kri05].

The algorithms presented in this paper can be used to predict the appearance of the fires produced by C-SAFE. These results are useful for understanding and explaining the simulations as well as for evaluating specific safety scenarios.

3.2. The Equation of Radiative Transfer

The evolution of radiance as light travels through a medium is defined by the Radiative Transport Equation (RTE). This integro-differential equation reads [SH81]

$$
\begin{aligned}
(\vec{\omega} \cdot \nabla) L(\lambda, \vec{x}, \vec{\omega}) = & -\sigma_a(\lambda, \vec{x}) \cdot L(\lambda, \vec{x}, \vec{\omega}) \\
& +\sigma_a(\lambda, \vec{x}) \cdot L_e(\lambda, \vec{x}, \vec{\omega}) \\
& -\sigma_s(\lambda, \vec{x}) \cdot L(\lambda, \vec{x}, \vec{\omega}) \\
& +\sigma_s(\lambda, \vec{x}) \cdot L_i(\lambda, \vec{x}, \vec{\omega}),
\end{aligned}
\tag{1}
$$

where L_i (in $\frac{J}{s \cdot m^2 \cdot sr \cdot nm}$) is defined as

$$
L_i(\lambda, \vec{x}, \vec{\omega}) = \int_{4\pi} L(\lambda, \vec{x}, \vec{\omega}_i) \cdot \Phi(\lambda, \vec{\omega}, \vec{\omega}_i) d\vec{\omega}_i.
\tag{2}
$$

The RTE states that the variation of the spectral radiance L, in the direction of interest $\vec{\omega}$, over a segment of infinitesimal length, is subject to the following phenomena :

- absorption : some photons traversing the medium will be absorbed proportionally to the absorption coefficient σ_a (in m^{-1}). This term also accounts for induced emission, which occurs when electrons in an excited state are induced by photons to drop to a lower energy state, emitting photons of similar wavelength in the process.
- emission : some photons will be emitted by the medium. These are represented by the emitted spectral radiance L_e.
- out-scattering : some photons initially traveling along the direction of interest $\vec{\omega}$ might be scattered in another direction when colliding with a particle. This effect is characterized by the scattering coefficient σ_s (in m^{-1}).
- in-scattering : some photons initially traveling along an arbitrary direction $\vec{\omega}_i$ might be scattered in the direction of interest. The amount of photons subject to this process is represented by the in-scattering radiance L_i.

While the absorption and scattering coefficients depend only on the wavelength λ and position in space $\vec{x}$, the radiance is also dependent on the direction of interest $\vec{\omega}$. See [Pre03] for a broader description of the terms and their units.

Assuming that the properties of the participating medium are homogeneous over a small segment $\|\Delta\vec{x}\|$ in space, an analytical solution to the RTE can be derived

$$
\begin{aligned}
L(\lambda, \vec{x} + \Delta\vec{x}, \vec{\omega}) = & \ e^{-\sigma_t(\lambda, \vec{x}) \cdot \|\Delta\vec{x}\|} \cdot L(\lambda, \vec{x}, \vec{\omega}) + \\
& (1 - e^{-\sigma_t(\lambda, \vec{x}) \cdot \|\Delta\vec{x}\|}) \cdot \\
& \frac{\sigma_a(\lambda, \vec{x}) \cdot L_e(\lambda, \vec{x}, \vec{\omega}) + \sigma_s(\lambda, \vec{x}) \cdot L_i(\lambda, \vec{x}, \vec{\omega})}{\sigma_t(\lambda, \vec{x})},
\end{aligned}
\tag{3}
$$

where the extinction coefficient σ_t is defined as $\sigma_t = \sigma_a + \sigma_s$.

3.3. Scattering

The spherical distribution of scattered light is defined by a phase function. Such a function was developed by Henyey-Greenstein [HG41], and has been widely used in computer graphics. It is defined by a single asymmetry coefficient g controlling the distribution of the scattered light, and reads

$$\Phi_{HG}(\lambda, \vec{\omega}, \vec{\omega}_i) = \frac{1}{4\pi} \cdot \frac{1 - g(\lambda)^2}{(1 + g(\lambda)^2 - 2g(\lambda)\vec{\omega} \cdot \vec{\omega}_i)^{\frac{3}{2}}}, \quad (4)$$

where g can be a function of wavelength, although in most applications it is chosen to be constant. This value must be in the range (-1, 1), where g<0, g=0 and g>0 correspond respectively to backward, isotropic and forward scattering. See [Pre03, PH04] for more details on phase functions.

[DMB94, ZCMG00, KLF01] report low albedo values for several types of fuels, where the albedo ω is defined as σ_s/σ_t. Consequently, in a low-albedo medium such as the flames of interest, absorption usually dominates largely over scattering which contributes very little to the final image.

Moreover, [WCMB03] provides forward angle scattering ratios and asymmetry ratios for several types of aerosols and smoke particles produced by different fuels. Those ratios indicate strongly forward dominated scattering distributions for almost all the reported types of particles. The larger the ratios are, the closer to one the value of g will be. This translates into a further diminishing impact of the scattering phenomenon which tends towards an unscattered distribution where the photons continue along their initial directions.

Finally, equation 3 is suitable for ray integration as all terms can be simply evaluated along the direction of interest, with the exception of L_i which implies the computation of an integral over the sphere, hence requiring Monte Carlo or other expensive approximation techniques. For these reasons, we will ignore scattering effects and focus on absorption and emission phenomena in the remaining of this paper.

3.4. Spectral Properties of Soot

For most fires, the light generated is dominated by emissions from soot particles. Soot emits a continuous spectrum in the visible range and often doubles or triples the radiation emitted by the gaseous products only [SH81]. The radiative properties of soot are a function of the soot concentration and the optical constants n and k of the particle. n and k are respectively the real and imaginary parts of the complex index of refraction $\bar{n} = n - ik$, which depends on the soot chemical composition. Although n and k are somewhat wavelength dependent, they are very weakly dependent on temperature. The spectral absorption coefficient is estimated as [DS69]

$$\sigma_a(\lambda) = f_v \cdot \frac{36\pi}{\lambda^{\alpha(\lambda)}} \cdot \frac{nk}{(n^2 - k^2 + 2)^2 + 4n^2k^2}. \quad (5)$$

The soot volume fraction, meaning the volume of soot particles per unit volume of cloud, can be evaluated as

$f_v = N \cdot \frac{4}{3}\pi R^3$, where N is the number density (number of particles per unit volume) and R is the radius of a soot particle (assumed to be spherical). [DS69] also provides values of n and k in the visible range for different types of soot. In the visible range, [Hot54] recommended the value $\alpha(\lambda) = 1.39$.

3.5. Black Body Radiation

In a medium where local thermodynamic equilibrium (LTE) prevails, which is an accurate assumption for fires, all the radiation can be assumed to result from thermal agitation, which is directly indicated by the medium's temperature [RHC95]. Indeed, in most fires, visible radiation is dominated by LTE radiation from soot particles. Blackbody radiation is described by Planck's formula which characterizes the emitted spectral radiance ($\frac{J}{s \cdot m^2 \cdot sr \cdot nm}$)

$$B_\lambda(T, \lambda, n) = b_\lambda(\lambda) \cdot \frac{1}{e^{\frac{hc}{\lambda kT}} - 1} = \frac{2hc^2}{\lambda^5} \cdot \frac{1}{e^{\frac{hc}{\lambda kT}} - 1} \quad (6)$$

as a function of temperature T, wavelength λ, and index of refraction n defining the speed of electromagnetic propagation $c = c_0/n$ in the medium. The remaining constant terms are Boltzmann constant k, Planck's constant h, and the speed of electromagnetic propagation in a vacuum c_0.

3.6. Spectral Properties of other Chemical Species

Computing the energy states of a molecule, which are needed to predict its spectral properties, implies solving the Schrödinger equation. In the case of the simple Hydrogen atom where a single electron orbits around the nucleus, it is possible to analytically derive an expression describing the energy levels. However, for more complex atoms or molecules, closed forms do not exist and intense computations are required to evaluate numerical approximations of the quantum energy eigenstates and eigenvalues.

Given the complexity of solving this equation, we chose instead to utilize tabulated spectral properties based on experimental data. In the case of atoms, such a compilation is made publicly available through the NIST Atomic Spectra Database [Ral96, NA]. With respect to molecules, the HITRAN Molecular Spectroscopic Database [Rea05, HIT] provides spectral measurements for several common species.

While an atomic radiation of frequency ν is exclusively produced by an electronic transition from an upper state of energy E_2 to a lower state E_1 such that $\Delta E = E_2 - E_1 = h\nu$ as stated by Planck's law, molecules can also radiate due to vibrational or rotational transitions. However, vibrational and rotational transitions usually occur in the infrared and radio range respectively. The emission coefficient ($\frac{1}{m} \cdot \frac{J}{s \cdot m^2 \cdot sr \cdot nm}$) and absorption coefficient associated to a spectral line of frequency $\nu = c/\lambda$ can be computed as [Rea98, MW06]

$$j_\lambda = \frac{h\nu}{4\pi} N_2 A_{21} \phi(\lambda), \quad (7)$$

$$\sigma_a = \frac{h\nu}{4\pi}(N_1 B_{12} - N_2 B_{21})\phi(\lambda), \quad (8)$$

where N_1 and N_2 represent the number density of elements (atoms or molecules) in the lower and upper state respectively, and $\phi(\lambda)$ is the normalized spectral line shape. A_{21}, B_{21} and B_{12} are the Einstein coefficients measuring the transition probabilities of spontaneous emission, induced emission and absorption respectively. More specifically,

- A_{21} gives the probability per unit time that an electron in an upper energy orbital will decay spontaneously to a lower energy orbital, releasing a photon in the process
- B_{21} gives the probability per unit time per unit energy density of the radiation field of an electron in an upper energy orbital being induced to decay to a lower energy orbital in presence of an electromagnetic radiation near the frequency of the transition, releasing a photon in the process
- B_{12} gives the probability per unit time per unit energy density of the radiation field of an electron in a lower energy orbital jumping to a higher energy orbital in presence of an electromagnetic radiation near the frequency of the transition, absorbing a photon in the process

The Einstein coefficients are fixed probabilities associated with each element, and do not depend on the state of the gas of which the elements are part. They are related by [Mod03]

$$\frac{A_{21}}{B_{21}} = b_\lambda(\lambda) \quad and \quad \frac{B_{21}}{B_{12}} = \frac{g_1}{g_2}, \tag{9}$$

where g_i is the degeneracy of state i, or the number of states having the same energy level. Assuming local thermodynamic equilibrium, the population partition at temperature T between states is governed by the Maxwell-Boltzmann distribution [Mod03]

$$\frac{N_i}{N} = \frac{g_i \cdot e^{-\frac{E_i}{kT}}}{Z(T)}. \tag{10}$$

This distribution states that the population of a given state decays exponentially with its energy, the temperature modulating the rate of decay. The partition function is given by

$$Z(T) = \sum_j g_j \cdot e^{-\frac{E_j}{kT}}. \tag{11}$$

Combining the previous equations yields a formula to compute the absorption coefficient as

$$\sigma_a = \frac{\phi(\lambda)}{8\pi} N_2 A_{21} \frac{\lambda^4}{c} (e^{\frac{hc}{\lambda kT}} - 1), \tag{12}$$

as well as Kirchoff's law which allows to compute the emission coefficient as $j_\lambda = \sigma_a \cdot B_\lambda(T, \lambda) = \sigma_a \cdot L_e$.

3.7. Refraction

Photons traversing a fire might follow non-linear trajectories due to the spatially varying refractive properties, inducing the wavy visual feedback that an observer might experience as looking through a flame. While the refractive properties of a fire have a small effect for still images, this effect becomes important when observing an animated sequence.

It is possible to approximate the indices of refraction in the medium by simply computing the refractive indices of air. For this purpose, Ciddor's equation [Cid96] is believed to provide accurate results over a broad range of wavelengths and under extreme environmental conditions of temperature, pressure, and humidity. For this reason, it has been adopted by the International Association of Geodesy (IAG) as the standard equation for calculating index of refraction.

Given an incident ray from a medium of index η_i of angle θ_i with the normal, being refractively transmitted into a medium of index η_t with an angle θ_t, Snell's law states that $\eta_i \sin \theta_i = \eta_t \sin \theta_t$. Figure 2 shows a scene where the refractive properties of the flame were included in the rendering.
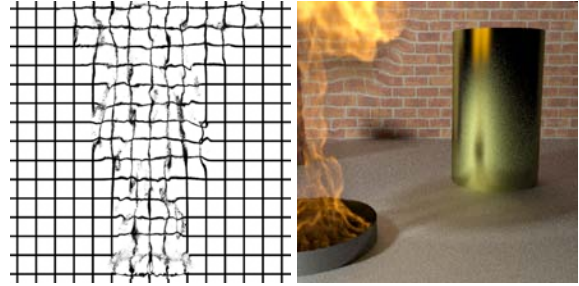

Figure 2: *Modeling of the refractive properties: refraction field only (left) and a scene where the refraction process induces the warping of the background brick pattern and slight caustics on the floor near the flame envelop (right) with increased index of refraction to better exhibit the deformation*

3.8. Visual Adaptation

The biological elements constituting the visual system of a human being present an extremely complex structure. As such, the signal they emit in response to a given intensity input obeys various intricate mechanisms notoriously hard to model, but which must be considered in order to carry a high fidelity rendering process. The previous statement is even more valid in the case of flame rendering than for usual scenes because of their high dynamic range nature. This is due to the fact that the cones which are responsible for the color vision in the photopic range display S-potential responses, as first investigated by [NR66]. Based on studies of photoreceptor response, Naka and Rushton proposed a simple function to describe the response generated by the retinal photoreceptors to an input intensity L

$$R(L, \sigma) = \frac{L}{L + \sigma}. \tag{13}$$

This non-linear response depends on an adaptation state σ determined by the visual system to maximize the perception of features for a given scene. For a constant adaptation level, the curve displays a sigmoidal shape on a logarithmic scale, and explains why a flame looking yellow-white when observed at night might appear orange-yellow in a sunlight illuminated environment, as reproduced in Figure 3.

Figure 3: *Modeling the adaptation of the visual system allows for a faithful reproduction of the colors observed when looking at a flame under different lighting conditions*

This model was the precursor to numerous more complex methods [DCWP02]. Models such as [FPSG96, PTYG00] also consider the grey-scale response provided by the rods in the scotopic range along with the associated loss of visual acuity, the latter defining the ability to resolve spatial details. However, flames are luminous objects which will always fall in the photopic range of the visual system. For this reason, scotopic range phenomena can be safely ignored.

4. Implementation

The rendering process has been integrated in a path-tracer which allows for the global illumination of a potential scene by the fire. The data are represented by a set of volumes describing the fields of interest, such as temperature, pressure, and concentration of the different chemical species. The evolution of the radiance along a ray is integrated using equation 3 in a ray-marching algorithm where the properties of the medium are assumed to be constant along a small segment in space. This assumption is justified by the fact that we can set the length of a segment to be arbitrarily small, providing a tradeoff of quality versus rendering time.

Our path-tracer provides support to model scattering properties via the implementation of a Monte-Carlo integration method which offers computationally expensive but accurately converging solutions. However, for the reasons described in section 3.3, the majority of our renderings were generated without scattering effects, hence setting $\sigma_s = 0$.

The volume containing the spectral absorption coefficients is precomputed using equations 5, 12 and 10 as the databases used provide the values of the wavelength λ of the spectral lines along with the associated Einstein coefficient A_{21}, and degeneracy g_2 and energy value E_2 of the excited state. These are simply added together for the different species, even though a more precise method using a spectral overlap correction term could be used [Jon00]. The HITRAN Molecular Spectroscopic Database directly provides values of the partition function as a function of temperature for each species. When using data from the NIST Atomic Spectra Database, the value of the partition function can be computed using equation 11. Since we use a

discretized representation of the visible spectral domain, we define $\phi(\lambda) = 1/SpectralBinWidth$. The emitted spectral radiance is computed by means of equation 6 using the temperature field while ray-marching.

Even though methods such as [SL96] would remove aliasing, the non-linear trajectory followed by photons due to the refractive properties of the medium is evaluated by using an extension of [BTL90] which is more suitable for ray-marching. In order to lower aliasing, the gradient of the refractive index field is computed at each ray-marching step by applying central differences at the projection of the current location onto the boundaries of the voxel for each axis, and linearly interpolating the resulting values. The gradient is then considered to be the normal of the dielectric layer with which the ray interferes, and geometric perturbations of the path are computed according to Snell's law.

The reproduction of the visual adaptation process has been implemented as a post-rendering step. Due to the limitations of the RGB color space, the radiance spectra are instead converted to the XYZ color space using the tristimulus curves defined by the Commission Internationale de l'Eclairage (CIE). This step can actually be processed either after solving for the radiance terms using a fully spectral representation, or before, which considerably reduces the computational cost and most often provides a visually accurate approximation. Those values are then converted into the LMS cone response domain where the tone-mapping operator described in equation 13 is applied. At this step, the derivation of the adaptation state σ can be computed as in [IFM05], or even adjusted in order to simulate effects such as temporal light adaptation. In our implementation, we simply evaluate σ based on the average of the LMS cone response values throughout the image. A final conversion to the RGB color space allows for gamma correction and display.

5. Results

To evaluate its robustness, we applied our technique to several data sets. Figure 1 and 4 show the rendering of various types of fires typically dominated by soot radiation. Figure 5 shows a side by side comparison of some photographs and renderings of spectroscopy experiments using chemical elements with very characteristic spectral signatures.

These renderings were generated in 40 to 80 seconds each on a dual Intel Xeon 3.00GHz processor desktop using one sample per pixel and 512^2 pixels. The volumes have resolutions varying from 200^3 to 300^3, and the ray-marching step was set to a half of the size of a voxel. When accounting for the refractive properties of the medium, the rendering time increases by a factor of about 1.25. The preprocessing stage, which consists in integrating the absorption coefficient throughout the volume, requires from a few minutes to about an hour on a single processor, depending on the complexity of the spectral properties of the chemical species of interest. Because of the simple analytical equations governing the

spectral properties of soot, the preprocessing stage reduces to a few seconds when considering radiation from soot only.
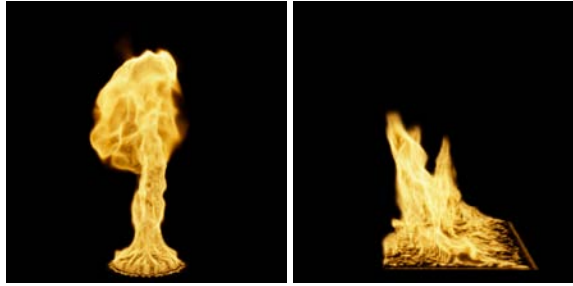

Figure 4: *Renderings of fires typically dominated by the radiation from soot particles : a heptane pool fire (left) and a simulation of a JP-8 bonfire with lateral crosswind (right)*
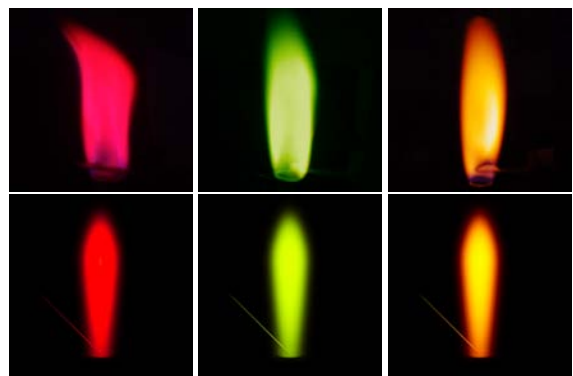

Figure 5: *Comparison of actual pictures (top) and renderings (bottom) of spectroscopy experiments with various chemical species : Lithium, Barium and Sodium*

6. Conclusion and Future Work

We have presented a new robust physically-based realistic fire rendering algorithm which employs detailed simulation of the radiative emission and refractive transfer occurring in real flames as well as a biologically-based model of the visual adaptation phenomenon. These are the key-components to the highly realistic renderings achieved by our method. This model also aims at filling the gap currently existing in the literature with respect to the rendering of colorful flames, since it accommodates fires dominated by the radiation from any combination of chemical species.

However, our model is inherently sensitive to the richness of the database used for each chemical species other than soot. Moreover, our model has only been validated in a qualitative manner, and we feel that a rigorous evaluation of its accuracy, by comparing predictions built on experimental data against measured radiances, would give focus to a future direction of research. We also wish to extend this work to plasma rendering, the later being a gas of extremely high temperature inducing ionization of its constitutive elements.

References

[AH05] ADABALA N., HUGHES C. E.: Gridless controllable fire. *Game Programming Gems 5* (2005), 539–549.

[BLLR06] BRIDAULT-LOUCHEZ F., LEBLOND M., ROUSSELLE F.: Enhanced illumination of reconstructed dynamic environments using a real-time flame model. *Afrigraph* (2006), 31–40.

[BPP01] BEAUDOIN P., PAQUET S., POULIN P.: Realistic and controllable fire simulation. *Graphics Interface* (2001), p159.

[BS97] BUKOWSKI R., SÉQUIN C.: Interactive simulation of fire in virtual building environments. *SIGGRAPH* (1997), 35–44.

[BTL90] BERGER M., TROUT T., LEVIT N.: Ray tracing mirages. *IEEE Comp. Graph. and Appl. 10*, 3 (1990), 36–41.

[Cha02] CHALMERS A.: Very realistic graphics for visualising archaeological site reconstructions. In *SCCG* (2002), pp. 7–12.

[Cid96] CIDDOR P. E.: Refractive index of air: new equations for the visible and near infrared. *Appl. Optics 35* (1996), p1566.

[CMTM94] CHIBA N., MURAOKA K., TAKAHASHI H., MIURA M.: Two-dimensional visual simulation of flames, smoke and the spread of fire. *Jour. of Vis. and Comp. Anim. 5*, 1 (1994), 37–54.

[DC01] DEVLIN K., CHALMERS A.: Realistic visualisation of the pompeii frescoes. In *AFRIGRAPH* (2001), pp. 43–48.

[DCWP02] DEVLIN K., CHALMERS A., WILKIE A., PURGATHOFER W.: Tone reproduction and physically based spectral rendering. *State of the Art Reports, Eurographics* (2002), p101.

[DMB94] DOBBINS R. A., MULHOILAND G. W., BRYNER N. P.: Comparison of a fractal smoke optics model with light extinction measurements. *Atmos. Env. 28*, 5 (1994), 889–897.

[DS69] DALZELL W. H., SAROFIM A. F.: Optical constants of soot and their application to heat-flux calculations. *Journal of Heat Transfer 91* (1969), 100–104.

[ENM99] ENGELL-NIELSEN T., MADSEN S. T.: Modelling, animation & visualisation of fire. *Master Thesis* (1999).

[FOA03] FELDMAN B. E., O'BRIEN J. F., ARIKAN O.: Animating suspended particle explosions. *ACM Trans. Graph. 22*, 3 (2003), 708–715.

[FPSG96] FERWERDA J. A., PATTANAIK S. N., SHIRLEY P., GREENBERG D. P.: A model of visual adaptation for realistic image synthesis. In *SIGGRAPH* (1996), pp. 249–258.

[Gro95] GROSSHANDLER W.: RADCAL: A narrow-band model for radiation calculations in combustion environment. *NIST Technical Note 1402* (1995).

[Has02] HASINOFF S. W.: Three-dimensional reconstruction of fire from images. *Master Thesis* (2002).

[HG41] HENYEY L. G., GREENSTEIN J. L.: Diffuse radiation in the galaxy. *Astrophysics Journal 93* (1941), 70–83.

[HIT] HITRAN: http://cfa-www.harvard.edu/HITRAN/.

[HK03] HASINOFF S. W., KUTULAKOS K. N.: Photo-consistent 3d fire by flame-sheet decomposition. *ICCV* (2003), 1184–1191.

[HMS*00] HENDERSON T. C., MCMURTRY P. A., SMITH P. J., VOTH G. A., WIGHT C. A., PERSHING D. W.: Utah Center for the Simulation of Accidental Fires and Explosions. *Computing in Science & Engineering 2*, 2 (2000), 64–76.

[Hot54] HOTTEL H.: Radiant heat transmission. *McAdams, W. (Ed.), Heat Transmission (3rd edition), Chap. 4* (1954).

[IFM05] IRAWAN P., FERWERDA J. A., MARSCHNER S. R.: Perceptually based tone mapping of high dynamic range image streams. In *Rendering Techniques* (2005), pp. 231–242.

[IK03] ILMONEN T., KONTKANEN J.: The second order particle system. *WSCG* (2003).

[IM04] IHRKE I., MAGNOR M.: Image-based tomographic reconstruction of flames. In *SCA* (2004), pp. 365–373.

[Ina90] INAKAGE M.: A simple model of flames. In *CG International* (1990), pp. 71–81.

[IR02] ISIDORO J., RIGUER G.: Texture perturbation effects. *ShaderX, Wordware Inc.* (2002), 91–108.

[Jon00] JONES H. R. N.: Radiation heat transfer. *Oxford Chemistry Primers* (2000).

[KBR*05] KRISHNAMOORTHY G., BORODAI S., RAWAT R., SPINTI J. P., SMITH P. J.: Numerical modeling of radiative heat transfer in pool fire simulations. *ASME (IMECE)* (2005).

[KLF01] KRISHNAN S. S., LIN K.-C., FAETH G. M.: Extinction and scattering properties of soot emitted from buoyant turbulent diffusion flames. *Journal of Heat Transfer 123*, 2 (2001), p331.

[Kri05] KRISHNAMOORTHY G.: Predicting radiative heat transfer in parallel computations of combustion. *Ph.D. thesis* (2005).

[KRS05] KRISHNAMOORTHY G., RAWAT R., SMITH P. J.: Parallel computations of radiative heat transfer using the discrete ordinates method. *Num. Heat Trans.: B: Fund. 47* (2005), 19–38.

[LF02] LAMORLETTE A., FOSTER N.: Structural modeling of flames for a production environment. *SIGGRAPH* (2002), p729.

[LKMD01] LEE H., KIM L., MEYER M., DESBRUN M.: Meshes on fire. *Eurogr. Work. on Comp. Anim. and Sim.* (2001), 75–84.

[MK02] MELEK Z., KEYSER J.: Interactive simulation of fire. *Pacific Graphics (Poster session)* (2002), 431–432.

[Mod03] MODEST M. F.: Radiative heat transfer, 2nd edition. *Academic Press* (2003).

[MW06] MARTIN W., WIESE W.: Atomic spectroscopy. *National Institute of Standards and Technology* (2006).

[NA] NIST-ASD: http://physics.nist.gov/PhysRefData/ASD/.

[NFJ02] NGUYEN D. Q., FEDKIW R., JENSEN H. W.: Physically based modeling and animation of fire. In *SIGGRAPH* (2002), pp. 721–728.

[NR66] NAKA K. I., RUSHTON W. A. H.: S-potentials from luminosity units in the retina of fish (cyprinidae). *Journal of Physiology 185* (1966), 587–599.

[Par82] PARAMOUNT: Star Trek II: The Wrath Of Kahn, Genesis Demo. *SIGGRAPH Video Review* (1982).

[PH04] PHARR M., HUMPHREYS G.: Physically based rendering: From theory to implementation. *Morgan Kaufmann* (2004).

[PP94] PERRY C. H., PICARD R. W.: Synthesizing flames and their spreading. *Eurogr. Work. on Anim. and Sim.* (1994), 1–14.

[Pre03] PREMOZE S.: Approximate methods for illumination and light transport in natural environments. *Ph.D. Thesis* (2003).

[PTYG00] PATTANAIK S. N., TUMBLIN J., YEE H., GREENBERG D. P.: Time-dependent visual adaptation for fast realistic image display. In *SIGGRAPH* (2000), pp. 47–54.

[Rac96] RACZKOWSKI J.: Visual simulation and animation of a laminar candle flame. *GKPO* (1996).

[Ral96] RALCHENKO Y.: NIST Atomic Spectra Database. *Mem. S.A.It. Suppl. 8* (1996).

[Rea05] ROTHMAN L. S., ET AL.: The HITRAN 2004 molecular spectroscopic database. *Journal of Quantitative Spectroscopy and Radiative Transfer 96* (2005), 139–204.

[Rea98] ROTHMAN L. S., ET AL.: The HITRAN molecular spectroscopic database and hawks (hitran atmospheric workstation) 1996 edition. *Jour. of Quan. Spec. and Rad. Tran. 60* (98), p665.

[Ree83] REEVES W. T.: Particle systems - a technique for modeling a class of fuzzy objects. *Trans. Graph. 2*, 2 (1983), 91–108.

[RHC95] RUSHMEIER H. E., HAMINS A., CHOI M. Y.: Volume rendering of pool fire data. In *IEEE Computer Graphics and Applications, 15(4)* (1995), pp. 62–66.

[Rob01] ROBERTS I.: Realistic modelling of flame. *Bachelor Thesis* (2001).

[SF93] STAM J., FIUME E.: Turbulent wind fields for gaseous phenomena. In *SIGGRAPH* (1993), pp. 369–376.

[SF95] STAM J., FIUME E.: Depicting fire and other gaseous phenomena using diffusion processes. *SIGGRAPH* (1995), p129.

[SH81] SIEGEL R., HOWELL J.: Thermal radiation heat transfer. *Hemisphere Publishing Corp.* (1981).

[Sim90] SIMS K.: Particle animation and rendering using data parallel computation. In *SIGGRAPH* (1990), pp. 405–413.

[SL96] STAM J., LANGUÉNOU E.: Ray tracing in non-constant media. In *Rendering Techniques* (1996), pp. 225–234.

[TTC97] TAKAHASHI J., TAKAHASHI H., CHIBA N.: Image synthesis of flickering scenes including simulated flames. *IEICE Trans. on Information Systems E80-D*, 11 (1997), 1102–1108.

[WCMB03] WEINERT D. W., CLEARY T. G., MULHOLLAND G. W., BEEVER P. F.: Light scattering characteristics and size distribution of smoke and nuisance aerosols. *IAFSS* (03), p209.

[WLMK02] WEI X., LI W., MUELLER K., KAUFMAN A.: Simulating fire with texture splats. In *VIS* (2002), pp. 227–235.

[ZCMG00] ZHU J., CHOI M. Y., MULHOLLAND G. W., GRITZO L. A.: Soot scattering measurements in the visible and near-infrared spectrum. *Combustion Institute, International Symposium on Combustion 1* (2000), 439–446.

[ZWF*03] ZHAO Y., WEI X., FAN Z., KAUFMAN A., QIN H.: Voxels on fire. In *VIS* (2003), p. 36.